THE JOURNAL OF BIOLOGICAL CHEMISTRY VOL. 284, NO. 9, pp. 5630–5636, February 27, 2009

p38 MAPK Is an Early Determinant of Promiscuous Smad2/3 Signaling in the Aortas of Fibrillin-1 (*Fbn1*)-null Mice*

Received for publication, September 8, 2008, and in revised form, December 8, 2008 Published, JBC Papers in Press, December 24, 2008, DOI 10.1074/jbc.M806962200

Luca Carta[‡1], Silvia Smaldone[‡1], Lior Zilberberg[§], David Loch[¶], Harry C. Dietz[¶], Daniel B. Rifkin[§], and Francesco Ramirez[‡2]

From the [‡]Department of Pharmacology and Systems Therapeutics and the Cardiovascular Institute, Mount Sinai School of Medicine, New York, New York 10029, the [¶]Departments of Pediatrics, Medicine, and Molecular Biology and Genetics and the Howard Hughes Medical Institute, Johns Hopkins University School of Medicine, Baltimore, Maryland 21205, and the [§]Department of Cell Biology, New York University School of Medicine, New York, New York 10016

Excessive transforming growth factor-β (TGF-β) signaling characterizes the progression of aortic aneurysm in mouse models of Marfan syndrome, a systemic disorder of the connective tissue that is caused by mutations in the gene encoding the extracellular matrix protein fibrillin-1. Fibrillin-1 mutations are believed to promote abnormal Smad2/3 signaling by impairing the sequestration of latent TGF-β complexes into the extracellular matrix. Here we report that promiscuous Smad2/3 signaling is the cell-autonomous phenotype of primary cultures of vascular smooth muscle cells (VSMC) explanted from the thoracic aortas of *Fbn1* mutant mice with either neonatal onset or progressively severe aortic aneurysm. This cellular phenotype was characterized in VSMC isolated from *Fbn1*-null (mgN/mgN) mice, which recapitulate the most severe form of Marfan syndrome. We found that loss of fibrillin-1 deposition promotes the production of intracellular reactive oxygen species and abnormal accumulation of phosphorylated TGF-β-activated kinase 1 and p38 MAPK, in addition to increasing the levels of endogenous phospho-Smad2. We showed that improper Smad2/3 signaling in *Fbn1*-null VSMC is in part stimulated by phospho-p38 MAPK, which is in turn activated in response to signals other than those mediated by the kinase activity of the ALK5 receptor. Consistent with these cell culture data, *in vivo* analyses documented that phospho-p38 MAPK accumulates earlier than phospho-Smad2 in the aortic wall of mgN/mgN mice and that systemic inhibition of phospho-p38 MAPK activity lowers the levels of phospho-Smad2 in this tissue. Collectively, these findings indicate that improper activation of p38 MAPK is a precursor of constitutive Smad2/3 signaling in the aortic wall of a mouse model of neonatal lethal Marfan syndrome.

Marfan syndrome (MFS[3]) is a systemic disorder of the connective tissue with predominant manifestations in the cardiovascular, musculoskeletal, and ocular systems (1). MFS is caused by heterozygous mutations that affect the structure or decrease the expression of fibrillin-1, the major constituent of extracellular microfibrils, with an average diameter of 10 nm (1–4). Fibrillin-rich microfibrils are widely distributed architectural components of the extracellular matrix (ECM) that impart specific physical properties to connective tissues, either as obligatory constituents of elastic fibers or as elastin-free assemblies (2–4). Contrary to the earlier suggestion that MFS pathogenesis is solely accounted for by the loss of connective tissue integrity, mouse models of MFS have revealed that mutations in the fibrillin-1 gene (*Fbn1*) also promote promiscuous activation of latent TGF-β with adverse consequences to cellular activities (1). Relevant to aortic aneurysm, abnormal Smad2/3 signaling has been associated with disease progression in mice lacking or underexpressing fibrillin-1, which die at postnatal days 10–14 (P10–P14) (mgN/mgN mice) and at 2–6 months of age (mgR/mgR mice), respectively, and in mice heterozygous for a missense mutation in fibrillin-1, which display vascular abnormalities that do not reach a clinical end point (C1039G/+ mice) (5–7). Importantly, TGF-β antagonism has recently been shown to mitigate aneurysm progression in C1039G/+ mice and in severely affected MFS children (8, 9).

Fibrillin-1 is a large, cysteine-rich glycoprotein that can interact with cell surface receptors, such as integrins $\alpha_v\beta_3/\beta_6$ and $\alpha_5\beta_1$, and other extracellular molecules, including latent TGF-β-binding proteins 1 and 4 (10–13). Interaction of fibrillin-1 with integrins is believed to modulate cell behavior and/or guide microfibril biogenesis, whereas association with latent TGF-β-binding proteins has been shown to promote the storage of latent TGF-β complexes in the ECM (1–4). Thus, it has been argued that fibrillin-1 mutations in MFS render latent TGF-β more prone to activation by destabilizing its interaction with the extracellular microfibrils (14). Activators of latent TGF-β complexes include reactive oxygen species (ROS), matrix metalloproteases, thrombospondin-1, and integrins (15–20). Once activated, TGF-β signals through serine/threo-

* This work was supported, in whole or in part, by National Institutes of Health Grant AR049698, the Howard Hughes Medical Institute, the William S. Smilow Center for Marfan Syndrome Research, the National Marfan Foundation, and the Drs. Amy and James Elster Research Fund. The costs of publication of this article were defrayed in part by the payment of page charges. This article must therefore be hereby marked "*advertisement*" in accordance with 18 U.S.C. Section 1734 solely to indicate this fact.

[1] Both authors contributed equally to this work.

[2] To whom correspondence should be addressed: Dept. of Pharmacology and Systems Therapeutics and the Cardiovascular Institute, Mount Sinai School of Medicine, One Gustave L. Levy Pl., Box 1603, New York, NY 10029. Tel.: 212-241-7237; Fax: 212-996-7214; E-mail: francesco.ramirez@mssm.edu.

[3] The abbreviations used are: MFS, Marfan syndrome; ECM, extracellular matrix; ROS, reactive oxygen species; VSMC, vascular smooth muscle cell(s); TGF-β, transforming growth factor β; FBS, fetal bovine serum; MAPK, mitogen-activated protein kinase; P*n*, postnatal day *n*.

nine kinase receptors (TGFBRII and ALK5) and intracellular Smad2/3, Smad4 protein complexes that translocate into the nucleus and bind specific DNA elements in cooperation with other transcription factors (21). TGF-β can also signal through MAPK-dependent pathways, and molecules that transduce MAPK signals can directly or indirectly influence Smad2/3 activity (22).

The present study was designed to identify other molecular determinants of aneurysm progression in MFS by examining primary vascular smooth muscle cell (VSMC) cultures explanted from the thoracic aortas of MFS-like mice. Our results demonstrate that Smad2/3 signaling is constitutively active in VSMC cultures from mgN/mgN, mgR/mgR, and C1039/+ mice. We also present *in vitro* and *in vivo* evidence indicating that p38 MAPK is an early contributor to promiscuous Smad2/3 signaling during aneurysm progression in *Fbn1*-null mice. These findings extend our understanding of the molecular events associated with aneurysm progression in MFS.

EXPERIMENTAL PROCEDURES

Primary VSMC Cultures—Primary VSMC strains were established after isolating the cells from the thoracic aortas of 10-day-old mgN/mgN mice, 5-month-old mgR/mgR mice, 9-month-old C1039G/+ mice, and the respective wild-type littermates (23, 24). Aneurysm progression in mgR/mgR and C1039G/+ mice was monitored by echocardiography prior to the isolation of VSMC (8). Primary VSMC were expanded on 100-mm Primaria Plates dishes (BD Biosciences) in 1× Dulbecco's modified Eagle's medium containing 10% fetal bovine serum (FBS; Hyclone, Logan, UT) and supplemented with streptomycin, penicillin, and fungizone; cell aliquots were frozen and stored in liquid nitrogen for subsequent use. VSMC purity (evaluated by immunostaining with anti-α-SMA antibody) was estimated to range between 70 and 80% in mgN/mgN and mgR/mgR cultures and between 50 and 60% in C1039G/+ cultures. Cells between passages 3 and 8 were employed in the experiments described in the present study.

Cell Transfections—Primary VSMC were seeded the day before transfection at a density of 7500 cells/cm^2 and then cultured in 2% FBS. Cells were transiently co-transfected with 400 ng of the TGF-β-responsive plasmid p3TP-Lux or $(CAGA)_{12}$MLP-Luc (kind gifts of Drs. Joan Massagué and Peter ten Dijke, respectively) (25, 26) and 1 ng of the control plasmid SV40:Renilla-Luc (Promega, Madison, WI) using Lipofectamine 2000 (Invitrogen) (27). In some experiments, p3TP-Lux was transiently co-transfected with a plasmid that expresses a dominant negative version of Smad3 (DN-Smad3) lacking the MH2 domain (27). In other transfection experiments, VSMC cultures were treated with 5 μM SB203580, 5 μM SP600125, 10 μM PD98059 (Calbiochem-EMD Biosciences, La Jolla, CA), or 1 μM SB431542 (Sigma); control samples were treated with an equal volume of DMSO (vehicle). Luciferase assays were performed 24 h after cell transfection, and the results were evaluated as previously described (27). In the RNA interference experiments, mutant VSMC were retrotransfected with 50 μM small interfering RNA specific for p38α MAPK (MAPK14) or nontargeting small interfering RNA (J-040125 and D-001810–01, respectively; Dharmacon-Thermo Fisher Scientific, Lafayette, CO) using Lipofectamine 2000 (Invitrogen). Twenty-four hours later, retrotransfected cells were cultured for an additional 2 days in Dulbecco's modified Eagle's medium containing 2% fetal bovine serum. Protein extracts were analyzed as described below. Statistical analyses were performed for all of the experiments using Student's *t* test, assuming a *p* value of $\leq$0.05 as significant.

Detection of ROS—Levels of intracellular ROS were assessed using a modification of the published protocols (28, 29). Briefly, subconfluent VSMC cultures were washed with phosphate-buffered saline at 37 °C and incubated for 10 min in the dark in a phosphate-buffered saline-based buffer containing 10 μM 2,7-dichlorofluorescein diacetate (Molecular Probes, Inc., Eugene, OR) and 5.5 mM glucose. This was followed by an additional 10-min incubation in Dulbecco's modified Eagle's medium containing 10% FBS, fixation in 4% paraformaldehyde, and viewing with a Zeiss LSM 410 confocal microscope (Carl Zeiss SMT Inc., Peabody, MA) at λ = 488 nm. The intensity of the fluorescent signal was measured in several randomly chosen fields (each containing a minimum of 30 cells) with the aid of the MetaMorph version 6.3 software (Molecular Devices, Sunnyvale, CA), and it was expressed as the average combined value of all fields. Statistical analyses were performed using Student's *t* test, assuming a *p* value of $\leq$0.05 as significant.

Immunoblots, Immunohistochemistry, and in Vitro Kinase Assay—VSMC were cultured for 4 days in 10% FBS and for 2 additional days in 2% FBS. In some experiments, the culture medium included MAPK or ALK5 inhibitors at the aforementioned concentrations or 1 μM diphenylene iodonium (Calbiochem-EMD Biosciences). Cell layers were scraped into ice-cold Tris-buffered saline solution (pH 7.4) and flash frozen in liquid nitrogen. Cell and tissue extracts were prepared and assayed for total protein content using the BCA kit (Pierce) (7). Protein extracts (10–25 μg/lane) were fractioned by 10% (w/v) SDS-PAGE and electroblotted onto an Immobilon-P membrane (Millipore, Billerica, MA). Membranes were incubated first with antibodies against phosphorylated TGF-β-activated kinase 1 (phospho-TAK1 (TGF-β-activated kinase 1)), phospho-Smad2, phospho-p38 MAPK, or phospho-ATF2 (1:1000 dilution; Cell Signaling Technology, Danvers, MA) and subsequently with biotin-labeled anti-rabbit IgG antibody (1:25,000 dilution; Jackson ImmunoResearch Laboratories, West Grove, PA) and horseradish peroxidase-conjugated Streptavidin (Millipore). Immunoreactive products were visualized by chemiluminescence using the ECL Plus kit (Amersham Biosciences), and their relative intensity was evaluated with the aid of Adobe Photoshop software (Adobe Systems Inc., San Jose, CA). To assay p38 MAPK activity *in vitro*, cell lysates from wild-type and mutant VSMC cultures were immunoprecipitated overnight at 4 °C with an immobilized anti-phospho-p38 MAPK monoclonal antibody (Thr-180/Tyr-182; Cell Signaling Technology). Immunoprecipitates were subsequently incubated for 30 min at 30 °C with 1 μg of recombinant ATF2 and 200 μM ATP as per the manufacturer's protocol. Products of the reaction were resolved by SDS-PAGE and immunoblotted with an antibody against phospho-ATF2 (Thr-71). Positive bands were visualized and quantified as described above. Statistical analyses in all

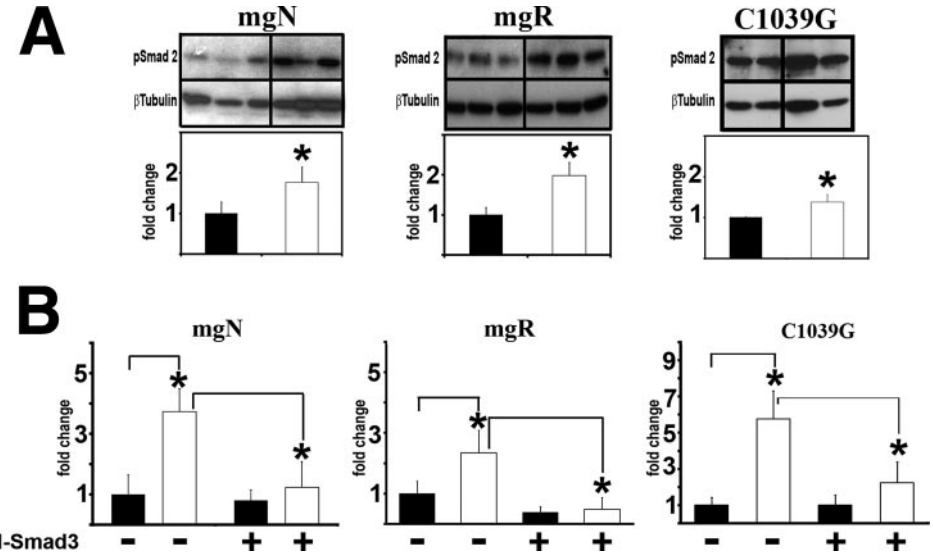

FIGURE 1. **Smad2/3 signaling is abnormally high in Fbn1 mutant VSMC cultures.** *A*, representative phospho-Smad2 immunoblots of protein extracts from VSMC cultures of the indicated genotypes ($n = 3$) with the *bar graphs below* summarizing the results of control (*black*) and experimental samples (*white*) normalized against β-tubulin levels. *B*, transcriptional activity of the p3TP-Lux reporter plasmid transiently transfected into VSCM of the indicated genotype ($n = 3$) without or together the DN-Smad3 expression plasmid. *Black* and *white bar graphs* summarize the results of three independent tests performed in duplicate for each of the experimental and control samples, respectively. In both *panels*, wild-type values are arbitrarily expressed as 1 unit, and *asterisks* indicate values statistically different from controls (Student's *t* test, $p \leq 0.05$).

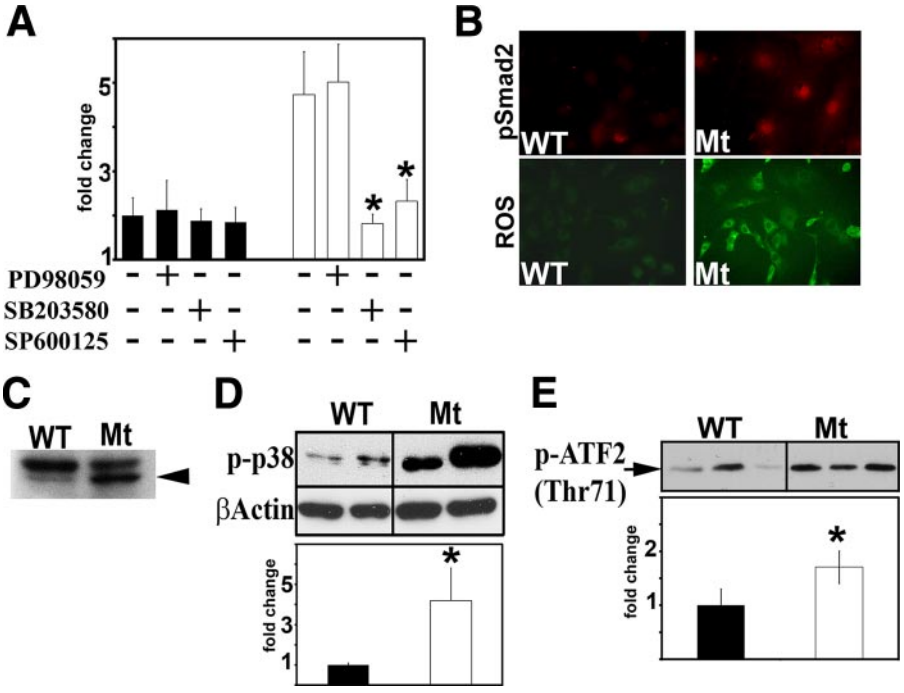

FIGURE 2. **Multiple signaling molecules are activated in Fbn1-null VSMC.** *A*, transcriptional activity of p3TP-Lux transfected into wild-type (*black*) or mgN/mgN (*white*) VSMC ($n = 3$) cultured with or without the indicated chemical inhibitors. The *bar graphs* summarize the results of three independent tests performed in duplicate for each of the experimental and control samples. *B*, immunodetection of phospho-Smad2 accumulation (*top*) and confocal microscopy of ROS production (*right*) in wild-type VSMC (*WT*) and 1106C cultures (*Mt*). In the latter sample, the intensity of the fluorescence signals in control and experimental samples were estimated to be 2,068.6 ± 332.1 and 3215.2 ± 957.3, respectively ($p = 0.0098$). *C*, representative immunoblot of phospho-TAK1 (*arrowhead*) in wild-type and 1106C cells. *D*, representative immunoblot of phospho-p38 MAPK (*phospho-p38*) in wild-type and 1106C cells. *E*, p38 MAPK-directed phosphorylation of ATF2 (pATF2) *in vitro* using protein extracts from wild-type and 1106 cells. The *bar graphs below* the immunoblots of *C* and *D* summarize the results of experimental (*white*) and control samples (*black*) normalized against β-actin levels and recombinant ATF2 input, respectively. The faster migrating band *highlighted* in the TAK1 immunoblot corresponds to the TAK1c/d isoforms (39). Experiments involving 1106C cells were each performed at least three different times. In relevant panels, wild-type values are arbitrarily expressed as 1 unit, and *asterisks* indicate values statistically different from controls (Student's *t* test, $p \leq 0.05$).

of these experiments were performed using the Student's *t* test, assuming a *p* value of ≤0.05 as significant. Tissue samples for immunohistochemistry were isolated from the thoracic aortas of wild-type and mgN/mgN mice, processed as previously described (7), and viewed with a Nikon Eclipse 80*i* microscope (Nikon Instruments Inc., Yokohama, Japan).

Experimental Animals—FR167653 (kindly provided by Astellas Pharma Inc., Tokyo, JP) was dissolved in saline solution containing 1% carboxymethylcellulose and administered to mgN/mgN mice and wild-type littermates ($n = 6$/genotype) by daily subcutaneous injections (from P1 to P10) at the dose of 32 mg/kg (30). An equivalent number of control mice was only treated with vehicle. Mice were sacrificed at P10 by carbon dioxide inhalation, and the thoracic aorta was transected, placed immediately in ice-cold Tris-buffered saline solution (pH 7.4), cleaned-up, and then flash frozen and stored in liquid nitrogen to be subsequently processed for protein analyses as described above. In parallel experiments, thoracic aortas from untreated wild-type and mgN/mgN mice sacrificed at P4 and P10 were similarly processed for protein analyses. All mouse experiments were approved by the Institutional Animal Care and Use Committee of the Mount Sinai School of Medicine.

RESULTS

Smad2/3 Signaling Is Constitutively Active in Fbn1 Mutant VSMC Cultures—Previous studies have associated the emergence of TGF-β-driven unproductive remodeling of the aortic wall with the progression of vascular disease in mice that harbor different *Fbn1* mutations and display discrete phenotypic outcomes (5–7). Here we evaluated TGF-β signaling (as evidenced by the accumulation of endogenous phospho-Smad2 and the transcription of TGF-β-responsive plasmids) in primary VSMC explanted from the thoracic aortas of these same

mutant animals (mgN/mgN, mgR/mgR, and C1039G/+ mice) that were sacrificed at comparable stages of aneurysm progression (10 days, 5 months, and 9 months of age, respectively) (5–7). The results demonstrated that all *Fbn1* mutant VSMC display higher levels of endogenous phospho-Smad2 and greater activity of transfected p3TP-Lux plasmid compared with the wild-type counterparts (Fig. 1, *A* and *B*). The latter observation was further validated by showing a significant reduction of p3TP-Lux activity in cells overexpressing DN-Smad3, a dominant-negative Smad3 protein that lacks the MH2 domain (Fig. 1*B*) (27). Identical results were obtained using the TGF-β-responsive plasmid $(CAGA)_{12}$MLP-Luc, (data not shown). Quantitative differences in Smad2/3 signaling between VSMC of different mutant genotypes and between individual cell strains of the same mutant genotype are likely to reflect variances in disease progression and penetrance (Fig. 1*A*). This last point notwithstanding, we concluded that primary VSMC cultures represent a suitable *in vitro* system to investigate abnormal signaling events associated with the deposition of a microfibril-deficient matrix.

Several Signaling Molecules Are Abnormally Activated in Fbn1-null VSMC—Cross-talk between TGF-β and MAPK-dependent pathways modulates cellular responses to specific stimuli (22). In order to verify whether MAPK-transduced signals contribute to elevated Smad2/3 activity in *Fbn1*-null VSMC, we compared luciferase expression of TGF-β-responsive plasmids transfected into wild-type or mutant cells that were cultured with or without the addition of chemical inhibitors of ERK (PD98095), p38 MAPK (SB203580), or JNK (SP600125). The choice of *Fbn1*-null cells was based on the assumption that the extremely rapid physical collapse of the aortic wall in mgN/mgN mice might eliminate the confounding effects of secondary cellular events that characterize late onset vascular disease in the other two mouse models of MFS (5–7). The results revealed that inhibition of either p38 MAPK or JNK activity negatively affects the expression of the p3TP-Lux and $(CAGA)_{12}$MLP-Luc reporter plasmids (Fig. 2*A*) (data not shown).

The present study focused on elucidating the causal relationship between p38 MAPK and TGF-β signaling. In order to maximize our read-outs, the analyses were performed using the *Fbn1*-null VSMC isolate with the highest levels of Smad2/3 signaling (strain 1106C). p38 MAPK has been implicated in transducing stress response signals as well as specific TGF-β stimuli that are mediated through the noncanonical TAK1 pathway (31–33). Similarly, TGF-β and stress response signals have been reported to promote ROS production, and ROS-elicited signals have been shown to stimulate TGF-β and phospho-p38 MAPK activity (29, 34). In line with these considerations, we found that 1106C cultures display increased nuclear localization of phospho-Smad2 as well as abnormally high levels of ROS, phospho-TAK1, and phospho-p38 MAPK (Fig. 2, *B–D*). Heightened p38 MAPK activity in *Fbn1*-null VSMC was independently confirmed by an *in vitro* assay that measured phosphorylation of the downstream effector ATF2 (Fig. 2*E*) (35). These observations therefore demonstrated that multiple signaling molecules are abnormally activated in primary VSMC cultures lacking fibrillin-1 microfibrils.

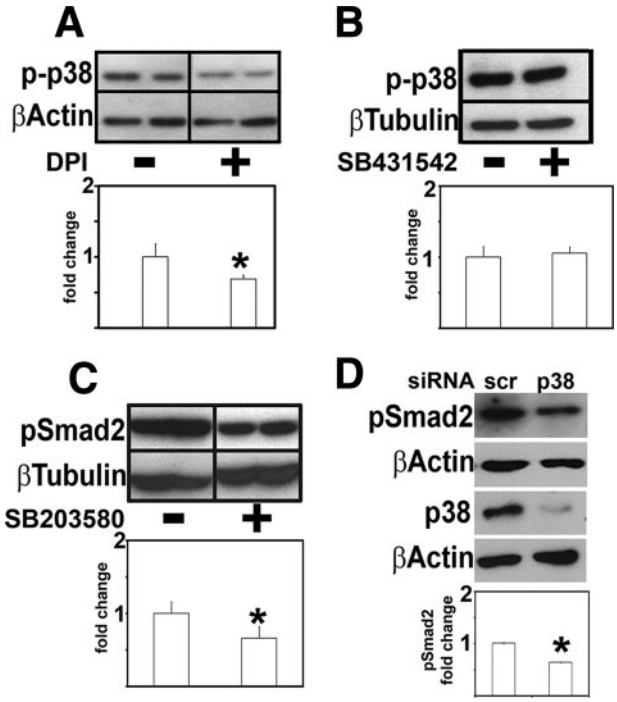

FIGURE 3. **p38 MAPK stimulates Smad2 in Fbn1-null VSMC.** Representative immunoblots of phospho-p38 MAPK (phospho-p38; *A* and *B*) and phospho-Smad2 levels (*C*) in 1106C cells cultured without (−) or with (+) the indicated inhibitors. *D*, representative immunoblots of phospho-Smad2 and p38 MAPK (p38) in 1106 cells retrotransfected with scramble (*scr*) or p38 MAPK small interfering RNAs. The *bar graphs* summarize the results of control and experimental tests, each performed three times. Data are normalized against β-tubulin or β-actin levels; control values are arbitrarily expressed as 1 unit, with *asterisks* indicating those statistically different from control samples (Student's *t* test, $p \leq 0.05$). *DPI*, diphenylene iodonium.

p38 MAPK Stimulates Smad2/3 Signaling in Fbn1-null VSMC—Next, chemical inhibitors were employed to assess the potential contribution of TGF-β-elicited signals to p38 MAPK stimulation and, implicitly, to phospho-p38 MAPK-driven Smad2/3 activation in 1106C cultures. In contrast to the ~35% decrease of phospho-p38 MAPK levels in mutant VSMC treated with the NADPH-oxidase inhibitor diphenylene iodonium (Fig. 3*A*), we found comparable amounts of phospho-p38 MAPK in 1106C cells cultured with or without the ALK5 kinase inhibitor SB431542 (Fig. 3*B*). Together, these results excluded a significant role of Smad-mediated signals in p38 MAPK activation. Surprisingly, the analyses also revealed that the p38 MAPK inhibitor SB203580 lowers the levels of endogenous phospho-Smad2 by ~30% (Fig. 3*C*), thus significantly less than the activity of the TGF-β-responsive plasmids (Fig. 2*A*). We believe that the discrepancy is likely to reflect experimental differences in the two assays and indirectly support this contention by noting that a different p38 MAPK inhibitor (FR167653) lowers phospho-Smad2 levels to the same extent as the SB203580 inhibitor both *in vitro* (data not shown) and *in vivo* (see below). Along the same lines, a ~30% reduction in phospho-Smad2 levels was also observed in *Fbn1*-null cells in which p38 MAPK production was nearly abrogated by RNA interference (Fig. 3*D*).

p38 MAPK Inhibition Decreases Smad2/3 Signaling in the Aortas of mgN/mgN Mice—The last set of experiments was designed to provide an *in vivo* validation of p38 MAPK role in promiscuous Smad2/3 signaling. Accordingly, phospho-p38

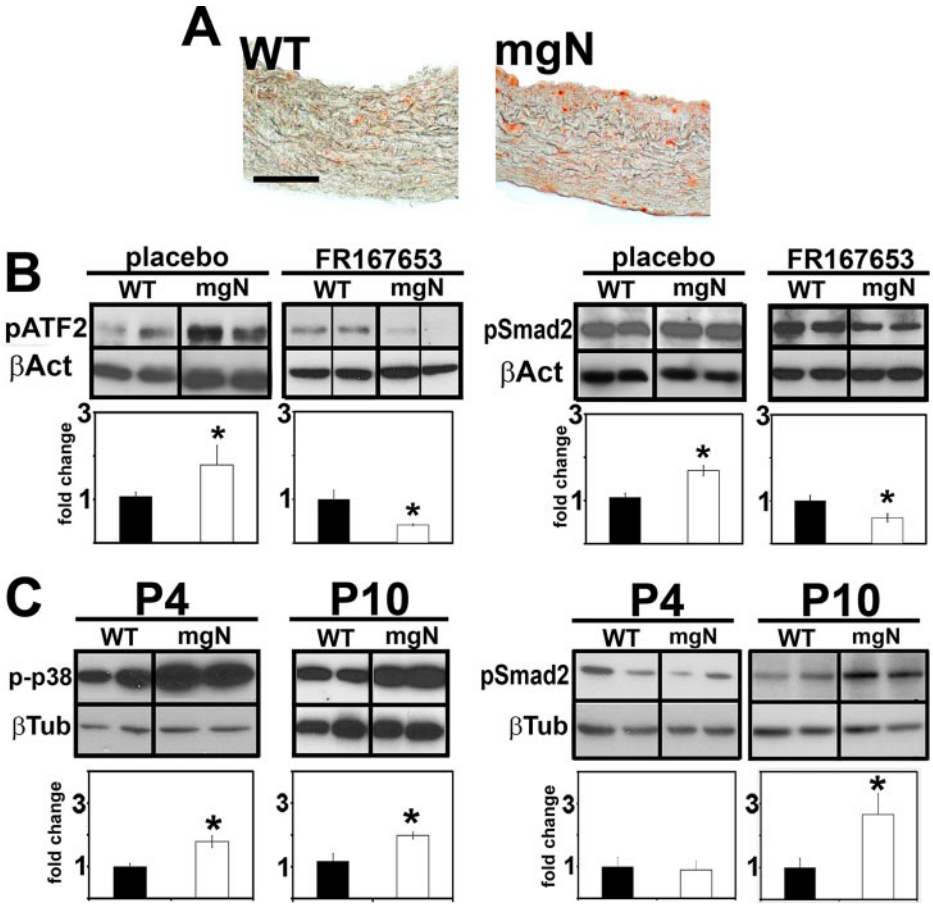

FIGURE 4. **p38 MAPK contributes to improper Smad2 signaling in mgN/mgN aortas.** *A*, thoracic aortas from P10 wild-type (*WT*) and *Fbn1*-null (*mgN*) mice immunostained for phospho-p38 MAPK. *Scale bar*, 50 μm. *B*, representative immunoblots of phospho-ATF2 and phospho-Smad2 in the thoracic aortas of wild-type or *Fbn1*-null mice ($n = 6$) treated with the phospho-p38 MAPK inhibitor or placebo. *C*, representative immunoblots of phospho-p38 MAPK (*phospho-p38*) and phospho-Smad2 in the thoracic aortas of untreated wild-type or *Fbn1*-null mice ($n = 6$) sacrificed at P4 or P10. The *bar graphs* in *B* and *C* summarize experimental (*white*) and control data (*black*) normalized against an internal control (β-tubulin or β-actin); wild-type values are arbitrarily expressed as 1 unit. The *asterisks* indicate values statistically different from those of control samples (Student's *t* test, $p \leq 0.05$).

MAPK levels were first shown to be abnormally elevated in the thoracic aortas of mgN/mgN mice (Fig. 4*A*). Next, p38 MAPK activity (as evidenced by the accumulation of the downstream effector phospho-ATF2 (35) and phospho-Smad2 levels were compared in the thoracic aortas of mgN/mgN mice and wild-type littermates, which had been systemically treated with the phospho-p38 MAPK inhibitor FR167653 from birth until P10 (30). The results of these *in vivo* inhibitions (summarized as relative protein ratios of experimental over control samples) demonstrated that treatment with FR167653 reduces the abnormal accumulation of phospho-Smad2 in the *Fbn1*-null aortas by ~30% (Fig. 4*B*). Last, Western blot experiments revealed a statistically significant increase of phospho-p38 MAPK in the thoracic aortas of untreated mgN/mgN mice earlier (P4) than phospho-Smad2 (P10) (Fig. 4*C*). Together, these *in vivo* data indicated that improper Smad2 stimulation in the aortic wall of mgN/mgN mice is temporally and causally related to p38 MAPK activation.

DISCUSSION

In vitro and *in vivo* experiments were performed to delineate the signaling profile of aneurysm progression in *Fbn1* mutant mice. These analyses have yielded two major new findings. First, they have documented that constitutive Smad2/3 signaling is maintained *in vitro* by VSMC explanted from the aortas of mice with different *Fbn1* mutations, phenotypic manifestations, and clinical outcomes. Second, they have demonstrated that abnormal p38 MAPK activation is an early contributor to Smad2/3 stimulation in the aortic wall of *Fbn1*-null mice. Together, these observations extend our understanding of the molecular events associated with aortic disease in MFS.

Previous studies of mouse models of MFS have demonstrated that connective tissue integrity and homeostasis depend on the threshold level of functionally competent microfibrils, which when it is breached by primary or secondary fibrillin-1 deficiencies triggers a destructive cascade involving unproductive tissue repair driven by dysregulated TGF-β activity (5–8, 14). Here we showed that the TGF-β-activated phenotype of aortas with structural, hypomorphic, or null mutations of *Fbn1* is replicated *in vitro* by the corresponding VSMC. Indeed, DNA microarray analyses have identified TGF-β as the only dysregulated pathway in common among these three mutant aortas.[4] These findings thus support the notion that constitutive activation of latent TGF-β is the common outcome of mutations that affect either the structure or the expression of fibrillin-1. Relevant to latent TGF-β activation, preliminary evidence suggests that one or more matrix metalloproteases are uphospho-regulated in *Fbn1*-null VSMC. *In vitro* retention of the TGF-β activated phenotype may in principle reflect a chronic response by the cultured cells to a structurally abnormal ECM, earlier developmental events that have altered cell fate, or a combination of both mechanisms. Ongoing studies are addressing these possibilities in VSMC from different *Fbn1* mutant mice as well as in cells derived from other mutant tissues.

The mgN/mN mice represent an informative model in which to investigate early events of dysregulated TGF-β activity in the diseased aorta (7). Although mgN/mgN aortas express molecular markers of TGF-β-driven tissue repair (7), loss of fibrillin-1 deposition leads to the extremely rapid physical collapse of the aortic wall without participation of

[4] L. Carta, unpublished results.

the destructive cascade that characterizes the progressively severe phenotype of mgR/mgR and C1039G/+ mice (5, 6). As such, early demise of mgN/mgN mice eliminates the problem of phenotypic heterogeneity noted in the other two MFS-like mice as they age. The downside of the *Fbn1*-null model is that potentially beneficial interventions can only be evaluated as changes in early molecular markers of disease progression rather than in improved aortic tissue architecture. With this limitation in mind, the study of cultured VSMC from mgN/mgN mice has revealed that loss of fibrillin-1 deposition elicits improper activation of several signaling molecules. We have examined the functional relationship between p38 MAPK and Smad2/3 because of the central role that the former molecule plays in multiple stress response pathways and in TGF-β signaling as well (31–33). Experiments using chemical inhibitors have documented the contribution of phospho-p38 MAPK to the transcription of TGF-β-responsive plasmids and to the accumulation of endogenous phospho-Smad2 in *Fbn1*-null VSMC. They have also demonstrated the ability of ROS but not ALK5 kinase to promote phospho-p38 MAPK accumulation. The latter finding is consistent with recent reports demonstrating that TGF-β activates c-Jun N-terminal kinase and p38 MAPK in an ALK5 kinase-independent manner (32, 33). It is also formally possible that activation of p38 MAPK in *Fbn1*-null VSMC cultures may be part of the stress response signals induced by impaired cell-matrix interactions. Irrespective of the underlying mechanism, our *in vivo* data indicate that phospho-p38 MAPK accumulates in the thoracic aortas of mgN/mgN mice before they progress to end-stage vascular disease, when heightened levels of phospho-Smad2 are first noticeable (7). Thus, we propose that loss of fibrillin-1 in mgN/mgN aortas promotes TGF-β- and/or ECM-mediated stimulation of p38 MAPK, and this in turn augments Smad2/3 signaling and perhaps induces TGF-β activators. Early activation of p38 MAPK and conceivably other MAPKs may also cooperate with Smad signaling in executing specific cellular programs that further contribute to aneurysm progression.

The discovery that TGF-β plays a central role in MFS pathogenesis has provided the rationale to explore therapeutic strategies against free TGF-β latent complex activators and/or Smad2/3 modulators (1). Although its precise mechanism of action is unknown, losartan has already proven to be an effective means to counteract TGF-β-driven manifestations in C1039G/+ mice and MFS children (8, 9). Consistent with earlier observations (5, 36), the matrix metalloprotease inhibitor doxycycline has also been shown to improve aortic wall architecture in C1039G/+ mice and delay aneurysm rupture in mgR/mgR mice (37, 38). The demonstration that p38 MAPK is implicated in constitutive activation of Smad2/3 signaling in the aortas of mgN/mgN mice points to another potential opportunity for therapy in MFS. Validation of this possibility, however, requires additional studies to establish whether p38 MAPK is also involved in the early stage of vascular disease in C1039G/+ and mgR/mgR mice or whether MAPKs are differentially activated in various mouse models of MFS.

Acknowledgments—We thank Dr. Lynn Sakai for invaluable comments, Drs. Joan Massagué and Peter ten Dijke for reagents, Sui Lee-Arteaga for technical support, and Karen Johnson for organizing the manuscript.

REFERENCES

1. Ramirez, F., and Dietz, H. C. (2007) *Curr. Opin. Genet. Dev.* **17,** 252–258
2. Kielty, C. M., Sheratt, M. J., and Shuttleworth, C. A. (2002) *J. Cell Sci.* **115,** 2817–2828
3. Ramirez, F., Sakai, L. Y., Dietz, H. C., and Rifkin, D. B. (2004) *Physiol. Genomics* **19,** 151–154
4. Hubmacher, D., Tiedemann, K., and Reinhardt, D. P. (2006) *Curr. Top. Dev. Biol.* **75,** 93–123
5. Pereira, L., Lee, S. Y., Gayraud, B., Andrikopoulos, K., Shapiro, S. D., Bunton, T., Biery, N. J., Dietz, H. C., Sakai, L. Y., and Ramirez, F. (1999) *Proc. Natl. Acad. Sci. U. S. A.* **96,** 3819–3823
6. Judge, D., Biery, N. J., Keene, D. R., Geubtner, J., Myers, L., Huso, D. L., Sakai, L. Y., and Dietz, H. C. (2004) *J. Clin. Invest.* **114,** 172–181
7. Carta, L., Pereira, L., Arteaga-Solis, E., Lee-Arteaga, S. Y., Lenart, B., Starcher, B., Merkel, C. A., Sukoyan, M., Kerkis, A., Hazeki, N., Keene, D. R., Sakai, L. Y., and Ramirez, F. (2006) *J. Biol. Chem.* **281,** 8016–8023
8. Habashi, J. P., Judge, D. P., Holm, T. M., Cohn, R. D., Loeys, B. L., Cooper, T. K., Myers, L., Klein, E. C., Liu, G., Calvi, C., Podowski, M., Neptune, E. R., Halushka, M. K., Bedja, D., Gabrielson, K., Rifkin, D. B., Carta, L., Ramirez, F., Huso, D. L., and Dietz, H. C. (2006) *Science* **312,** 117–121
9. Brooke, B. S., Habashi, J. P., Judge, D. P., Patel, N., Loeys, B., and Dietz, H. C. (2008) *N. Engl. J. Med.* **358,** 2787–2795
10. Sakamoto, H., Broekelmann, T., Cheresh, D. A., Ramirez, F., Rosenbloom, J., and Mecham, R. P. (1996) *J. Biol. Chem.* **271,** 4916–4922
11. Bax, D. V., Bernard, S. E., Lomas, A., Morgan, A., Humphries, J., Shuttleworth, C. A., Humphries, M. J., and Kielty, C. M. (2003) *J. Biol. Chem.* **282,** 34605–34616
12. Jovanovic, J., Takagi, J., Choulier, L., Abrescia, N. G., Stuart, D. I., van derMerwe, P. A., Mardon, H. J., and Handford, P. A. (2007) *J. Biol. Chem.* **282,** 6743–6751
13. Isogai, Z., Ono, R. N., Ushiro, S., Keene, D. R., Chen, Y., Mazzieri, R., Charbonneau, N. L., Reinhardt, D. P., Rifkin, D. B., and Sakai, L. Y. (2003) *J. Biol. Chem.* **278,** 2750–2757
14. Neptune, E. R., Frischmeyer, P. A., Arking, D. E., Myers, L., Bunton, T. E., Gayraud, B., Ramirez, F., Sakai, L., and Dietz, H. C. (2003) *Nat. Genet.* **33,** 407–411
15. Rifkin, D. B. (2005) *J. Biol. Chem.* **280,** 7409–7412
16. ten Dijke, P., and Arthur, H. M. (2007) *Nat. Rev. Mol. Cell Biol.* **8,** 857–869
17. Crawford, S. E., Stellmach, V., Murphy-Ullrich, J. E., Ribeiro, S. M., Lawler, J., Hynes, R. O., Boivin, G. P., and Bouck, N. (1998) *Cell* **93,** 1159–1170
18. Munger, J. S., Huang, X., Kawakatsu, H., Griffiths, M. J., Dalton, S. L., Wu, J., Pittet, J. F., Kaminski, N., Garat, C., Matthay, M. A., Rifkin, D. B., and Sheppard, D. (1999) *Cell* **96,** 319–328
19. Wipff, P. J., Rifkin, D. B., Meister, J. J., and Hinz, B. J. (2007) *Cell Biol.* **179,** 1311–1323
20. Jenkins, G. (2008) *Int. J. Biochem. Cell Biol.* **40,** 1068–1078
21. Shi, Y., and Massagué, J. (2004) *Cell* **113,** 685–700
22. Moustakas, A., and Heldin, C. H. (2005) *J. Cell Sci.* **118,** 3573–3584
23. Travo, P., Barrett, G., and Burnstock, G. (1980) *Blood Vessels* **17,** 110–116
24. Sprague, E. A., Kelley, J. L., and Schwartz, C. J. (1983) *Exp. Mol. Pathol.* **37,** 48–66
25. Wrana, J. L., Attisano, L., Carcamo, J., Zentella, A., Doody, J., Laiho, M., Wang, X. F., and Massagué, J. (1992) *Cell* **71,** 1003–1014
26. Dennler, S., Itoh, S., Vivien, D., ten Dijke, P., Huet, S., and Gauthier, J. M. (1998) *EMBO J.* **17,** 3091–3100
27. Zhang, W., Ou, J., Inagaki, Y., Greenwel, P., and Ramirez, F. (2000) *J. Biol. Chem.* **275,** 39237–39245
28. Bass, D. A., Parce, J. W., Dechatelet, L. R., Szejda, P., Seeds, M. C., and Thomas, M. (1983) *J. Immunol.* **130,** 1910–1917
29. Ohba, M., Shibanuma, M., Kuroki, T., and Nose, K. J. (1994) *Cell Biol.* **126,**

1079–1088
30. Ohashi, N., Matsumori, A., Furukawa, Y., Ono, K., Okada, M., Iwasaki, A., Miyamoto, T., Nakano, A., and Sasayama, S. (2000) *Artherioscler. Thromb. Vasc. Biol.* **20,** 166–172
31. Winter-Vann, A. M., and Johnson, G. L. (2007) *J. Cell Biochem.* **102,** 848–858
32. Sorrentino, A., Thakur, N., Grimsby, S., Marcusson, A., von Bulow, V., Schuster, N., Zhang, S., Heldin, C. H., and Landström, M. (2008) *Nat. Cell Biol.* **10,** 1199–11207
33. Yamashita, M., Faytol, K., Jin, C., Wang, X., Liu, Z., and Zhang, Y. E. (2008) *Mol. Cell* **31,** 918–924
34. Koli, K., Myllarniemi, M., Keski-Oja, J., and Kinnula, V. L. (2008) *Antioxid. Redox Signal.* **10,** 333–342
35. Morton, S., Davis, R. J., and Cohen, P. (2004) *FEBS Lett.* **13,** 177–183
36. Bunton, T. E., Biery, N. J., Myers, L., Gayraud, B., Ramirez, F., and Dietz, H. C. (2001) *Circ. Res.* **88,** 37–42
37. Xiong, W., Knispel, R. A., Dietz, H. C., Ramirez, F., and Baxter, B. T. (2008) *J. Vasc. Surg.* **47,** 166–172
38. Chung, A. W., Yang, H. H. C., Radomski, M. W., and van Breemen, C. (2008) *Circ. Res.* **102,** e73-e85
39. Watkins, S. J., Jonker, L., and Arthur, H. M. (2006) *Cardiovasc. Res.* **69,** 432–439